Nanoscale

MINIREVIEW

View Article Online
View Journal | View Issue

Cite this: *Nanoscale*, 2018, **10**, 19659

The wettability of gas bubbles: from macro behavior to nano structures to applications

Can Huang[a,b] and Zhiguang Guo *[a,b]

In recent years, various interfaces related to bubble wettability have been fabricated, which have already been widely applied in various disciplines and fields. Therefore, to better research and understand the wettability of gas bubbles, recent progress with interfaces and wettability of bubbles in aqueous media, including superaerophilicity and superaerophobicity, is summarized. Many biological interfaces which exhibit marvelous characteristics are discussed for reference. Because of the similar behavior between gas bubbles in aqueous media and droplets in air, the two wetting conditions are compared together to better illustrate theories of gas bubble wettability. Based on these theories, effective and available manipulation of gas bubbles' wettability provides a novel idea and method to solve practical problems in various aspects, *i.e.*, superaerophobic electrodes for gas evolution reactions, superaerophilic electrodes for gas compensation reactions, superaerophilic interfaces for directional collection and transportation of gas bubbles, and so on.

Received 8th September 2018,
Accepted 7th October 2018

DOI: 10.1039/c8nr07315e

rsc.li/nanoscale

1. Introduction

After billions of years, natural creatures have formed reasonably optimized composite structures and excellent wetting characteristics because of their continuous development and evolution on the earth. Composite structures with a macroscopic and microscopic combination show a stable compre-

[a]*Hubei Collaborative Innovation Centre for Advanced Organic Chemical Materials and Ministry of Education Key Laboratory for the Green Preparation and Application of Functional Materials, Hubei University, Wuhan 430062, People's Republic of China. E-mail: zguo@licp.cas.cn; Fax: +86-931-8277088; Tel: +86-931-4968105*
[b]*State Key Laboratory of Solid Lubrication, Lanzhou Institute of Chemical Physics, Chinese Academy of Sciences, Lanzhou 730000, People's Republic of China*

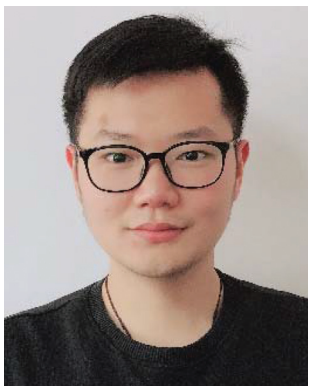

Mr Can Huang

Mr Can Huang joined Professor Guo's Biomimetic Materials of Tribology (BMT) group at Hubei University in 2017 to pursue his PhD degree. His current scientific interests are focused on surface wettability and researching potential applications.

Professor Zhiguang Guo

Professor Zhiguang Guo received his PhD from the Lanzhou Institute of Chemical Physics (LICP), Chinese Academy of Sciences (CAS), in 2007. After that, he joined Hubei University. From October 2007 to August 2008, he conducted his post-doctoral studies at the University of Namur (FUNDP), Belgium. From September 2008 to March 2011, he worked in the Funds for National Research Science (FNRS), Belgium, as a "Charge de Researcher". From February 2009 to February 2010, he worked in the Department of Physics, University of Oxford, UK, as a visiting scholar. Currently, he is a full professor at the LICP and is financed by the "Top Hundred Talents" program of the CAS. He has published more than 200 papers about the interfaces of materials.

hensive performance and unusual environmental adaptability. For example, the gliding of water striders without falling into the water,[1] the sucking up of water by beetles in a dry desert,[2] the persistent flying of termites in the rain,[3] the breathing of water spiders under water[4–6] and the "self-cleaning effect" of the lotus leaf surfaces,[7,8] and the formation of these amazing functions is related to the micro/nano hierarchical structure of legs, tails, wings, abdomens and leaves. Almost all the exceptional properties previously mentioned that are shown on the macro scale have microstructure support. In particularly, the "self-cleaning effect" of the lotus leaf surfaces is also known as lotus leaf effect or superhydrophobicity because of the nanostructures on top of the micro papillae.[9] Ultimately, the concepts of wettability derived from it are widely accepted.[10–21] In generally, the wetting in air is behavior that a solid interface is completely covered by another liquid.[8,22] In brief, the process of spreading of a liquid on a substrate is called wetting on the macroscopic scale. On the nanoscopic scale, when a solid substrate is wetted by a liquid, the liquid always spreads quickly on its surfaces. There is only has one contact point, solid/liquid, between them and some hydrophobic/superhydrophobic surfaces have three contact points solid/liquid, solid/gas and liquid/gas. It is worth mentioning that air bubbles have been found by researchers to have similar wettability under water. Another property of these hydrophobic/superhydrophobic surfaces is that they carry a gaseous plastron while being immersed in liquid. The gaseous plastron which is also called an air cushion is a thin air film between the substrates and the liquid. During the formation of the air film, the subaqueous surfaces seem to be wetted by air bubbles.[23] In fact, bubbles spreading on a superhydrophobic surface on a macroscopic scale can be seen as the complementary problem of wetting drops, where the two fluid phases have been exchanged.[24] The contact state between the substrates and liquid, which is the solid/liquid/gas three-phase contact state or solid/liquid two-phase contact state, is crucial to the behaviour of bubbles on substrates in liquid media on a nanoscopic scale.[25] Therefore, wettability/superwettability of gas bubbles is proposed, including aerophilicity, superaerophilicity, aerophobicity, and superaerophobicity.[26] The wettability of gas bubbles has attracted great attention because of its many potential applications and extensive fundamental research. Subsequently, more recently the behaviours of bubbles on substrates have taken on an important role in a wide range of scientific research and industrial applications especially in liquid media.[27–33] For example, the amount of air bubbles is a critical factor in electrochemical reduction. If too many bubbles are attached to the electrodes, which block the contact between the electrodes and the electrolyte, resulting in a remarkable reduction of the gas-evolution reaction (GER) efficiency.[22,34,35] However, too little bubble adhesion makes the gas-consumption reactions (GCRs) impossible. How to distribute the moderate bubbles evenly on the electrode interfaces is a critical step in determining the performances of various electrochemical reduction reactions of gas bubbles.[36–42] Fortunately, the "bubble bursting effect" and "the steady pinning effect of air bubbles" in nature set an example for the problems to be solved. Furthermore, an abundance of creatures show the behaviour of using bubble wettability in nature. In 2009, Jiang *et al.* discovered air bubbles quickly bursting within several milliseconds on a "self-cleaning" lotus leaf.[43] The phenomenon of the steady pinning effect of air bubbles on a rose petal with a combination of hierarchical rough structures was described in 2011.[25] Cerman *et al.* reported that Salvinia has a unique property drying in the water in 2009.[44] Therefore, some research and explorations of wetting interfaces have been developed and the various bio-inspired wettability surfaces have been prepared using this special property of gas bubbles. As described previously, the numerous reports of theoretical research and preparation methods of bubbles' wettability surfaces and their practical applications need a systematic and complete review. For interfaces in nature, especially, it is necessary and far-reaching to recognize and analyse them attentively from macro behaviours to nano structures and to imitate them.

The various interfaces in nature illustrate how the wettability of bubbles is used perfectly. The complementary roles of chemical component and interfacial structures on multiple scales are essential to this wettability. However, a few of these natural examples are presented separately in this review to illustrate and compare in detail different types of bubble wettability. In this review, some natural examples about the wettability of bubbles are summarized in detail to explain how organisms tactically use them to survive and adapt to the environment from the macro to the nano scales. At the same time, the wettability of bubbles under water is very similar, to a large extent, to the wettability of water drops in the air. Therefore, the theories relating to them in this review are put together for comparison and to better explain the wettability of bubbles. A numbers of fundamental and essential theories about the wettability of bubbles are explained. Furthermore, recent advances in the research on the wettability of bubbles, including how to design air bubble wettability by combining microstructures and chemical compositions of artificial interfaces and applications are discussed.

2. The wettability of bubbles from macro behaviour to nano structures in natural creatures

Abundant surfaces in nature, such as that of the lotus leaf, the wings of a butterfly, the legs of a water strider, and the compound eyes of mosquito, have attracted worldwide attention in recent decades in both academia and industry because of their extraordinary characteristics. In particular, the nano structures and macro behaviour of some plants and animals perfectly explain the wettability/superwettability of air bubbles. These examples have helped investigators better understand the mechanisms and processes of gas bubbles. Inspired by this, biomimetic material interfaces can be designed to meet

different needs. Therefore, it is essential that some examples are described in this review.

2.1 Rose petals

Rose petals have typical superhydrophobic surfaces which have a high water contact angle (WCA) of >150° and a low rolling angle of <10°, and this is well known by researchers. However, unlike ordinary superhydrophobic surfaces, rose petals also have a high adhesion to water droplets in the air, which is attributed to a combination of hierarchical rough structures (*i.e.*, micro-papillae and nano-folds). This phenomenon is defined as the "petal effect" (Fig. 1a).[49] In research, rose petals have not only been found to have an intriguing "petal effect", but also exhibit unique characteristics when immersed in an aqueous medium. Rose petals have an ability to trap air bubbles and rapidly stabilize them on its surfaces. This phenomenon is described as "the steady pinning effect of air bubbles".[25] Numerous studies have revealed that the rough micro/nano multi-layered composite structures of rose petals are crucial to this interesting property. Micro-sized rough protuberances and nano-papillae on the protuberance form an air cushion layer in the water environment. When bubbles approach the petal surfaces underwater, the air cushion induces the bubbles to merge into one, allowing the bubbles to be pinned on the petal surfaces. The macroscopic manifestation of this phenomenon is the CA hysteresis of the bubble, which makes it stick to the surface of the petals. It was found that petals stick to bubbles when they follow the Cassie model. Furthermore, the size of the micron scale protrusions and the interval between them are the main reason for determining the steady pinning effect of the air bubbles. Therefore, this bionic mechanism is widely used in the manufacture of various special surfaces. Thus, microstructures mainly affect the superhydrophobicity of rose petals, whereas the nanostructures are the key factor for the high adhesion to the rose petals.

2.2 Water spiders

The water spider (*Argyroneta aquatica*), is a unique spider that lives virtually its entire life under water.[4] Levi[5] found that the way they build underwater dwelling places, which are called diving bells, is amazing. The tough silk the water spiders spit out is not used to make a net, but is used to form a single, bell shaped dwelling in the water. In order to make the bell more solid and full, they use a special way to fill the diving bell full of air: they capture air at the surface of the water using the

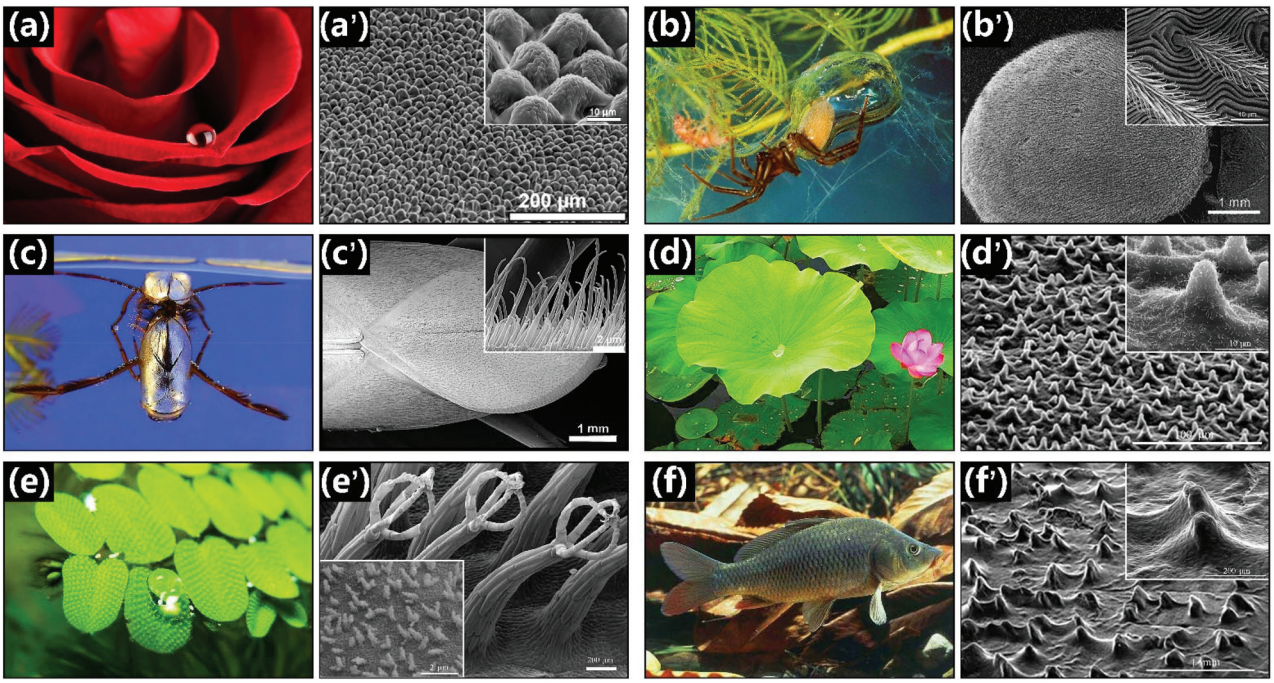

Fig. 1 The wettability of bubbles in natural creatures. (a) Based on hierarchical micro- and nanostructures, roses have a high adhesion and aerophobicity property, which is called steady pinning effect of air bubbles. Reproduced from ref. 43 with permission from *Thin Solid Films*, Copyright 2011. (b) The phenomenon of the earth's physical lung on water spiders with its superaerophilicity hairs of abdomen and legs. Reproduced from ref. 44 and 45 with permission from *SpringerPlus and Journal of Experimental Biology*. Copyright 2013. (c) Capturing the air by forming a shiny silvery film using multiple micro and nano superaerophilicity hairs of a water boatman. Reproduced from ref. 46 with permission from *Journal of Morphology*. Copyright 2011. (d) The phenomenon of lotus effect (*i.e.*, bubble-bursting performance) on Superaerophilic lotus leaves with micro-papillae and hydrophobic waxy nano-peaks. Reproduced from ref. 47 with permission from *ACS Applied Materials & Interfaces*. Copyright 2017. (e) A stable plastron is trapped on *Salvinia* under water because of its closed claw-like structures on the surfaces. Reproduced from ref. 48 with permission from *Advanced Materials*. Copyright 2010. (f) The scales of carp show good superaerophobicity in water. Reproduced from ref. 47 with permission from *ACS Applied Materials & Interfaces*. Copyright 2017.

hydrophobic hair on their abdomen and legs as shown in Fig. 1b and then climb back under the water to inject the air in the body of the diving bell. They repeat this behaviour more than once to make sure that they can survive safely and for a prolonged time underwater. This discovery was reported by Messner and Adis in 1995.[6] It is worth mentioning that the hairs, which have many nanometre-sized vertical dendritic structured layers, and the regular arrangement on the abdomen of water spiders are superaerophilic, which is the key factor that makes them able to easily collect air.[44] When a water spider is immersed in water, this special micro/nano multi-layered structure forms a thin film of air on the surfaces of its abdomen, which looks like a wrapping around the surface, giving it the function of transporting and storing air. This behaviour perfectly utilizes and interprets the wettability of bubbles under water.

2.3 Water boatman

The water boatman (*Notonecta glauca*) has two pairs of wings, anterior wings and posterior wings. The posterior wings which are membranous hide under the anterior wings. Sometimes the water boatman rises to the water surfaces to breathe, sometimes it sinks to the bottom of the water to avoid predators, and it can move very quickly. When the water boatman dives down to the bottom, there is a silvery shiny air film on the edge of its wings as shown in Fig. 1c. The existence of the air film is because of the excellent superhydrophobic properties of the surfaces of the posterior wings and the presence of numerous curving hairs. The formation of the superaerophilicity properties is related to the micro/nano composite structures of the wings' surfaces. These multilayer composite structures enable the boatman to capture large volumes of air in its wings and numerous curving micro-sized hairs. It is able to exhibit these properties under water because superhydrophobic surfaces become superaerophilic after being immersed in water. However, unfortunately the silvery shine of the air film is not stable for very long.[45,46,50]

2.4 Lotus leaf

The self-cleaning effects of plants have intrigued researchers over the past few decades. The lotus leaf is an outstanding example of this type of characteristic and has good development potential and prospects. In 1997, Barthlott[7] and Neinhuis[51] proposed the "lotus effect" and in their continued research concluded that its self-cleaning properties were the result of its microstructures and waxy materials as shown in Fig. 1d. Subsequently, the combination of micro/nano hierarchical structures on the lotus leaf surfaces and nanostructures on top of micro papillae were discovered by Feng *et al.* and they finally discovered that the hierarchical micro/nanostructures considerably increased the CA and decreased the sliding angle, which are the crucial factors in giving the lotus leaf, low adhesion, superhydrophobicity, and self-cleaning properties.[8] Nevertheless, the phenomenon of an air bubble bursting on a lotus leaf surface was first observed in 2009 by Jiang *et al.*,[43] which was described as the "bubble bursting effect". Similar to the wetting phenomena of water droplets in an air environment, the bubbles quickly spread and wetting its surfaces.[23] In fact, the spreading of air bubbles on lotus leaf surfaces can be seen as the wetting of droplets on its surfaces and the difference between them is that the gas phase and the liquid phase are exchanged.[24]

2.5 Salvinia

The floating water fern, *Salvinia molesta* has been so called because of its pinnate leaves. When immersed in water, its surfaces maintain a stable layer of air. Unlike other organisms that only maintain the air layers temporarily, *S. molesta* offers a novel mechanism for long-term air retention. Researchers found that the hierarchical architecture of the leaf surface is dominated by complex elastic eggbeater shaped hairs coated with nanoscopic wax crystals as shown in Fig. 1e. These special structures are the key factor for supporting the air–water interfaces to keep the air layers stable. This magical phenomenon is known as the "Salvinia effect". The unique combination of hydrophilic patches on superhydrophobic surfaces provides a promising concept for the development of a coating with long-term air retention properties.[48] This special structure of the natural interface has the characteristics of being superaerophilic, and is able to capture a certain amount of air by utilizing the wettability of the bubbles in the water.

2.6 Carp

Most fish have fish scales, and carp, as a species of fish, has a very smooth and layered small scale, as shown in Fig. 1f. These symmetrical and ordered scales not only enable the carp to move rapidly under water, but also to have excellent antifouling properties because of the superoleophobic interface with the water.[52] In reality, the surfaces of the fish scales are superhydrophilic, which is attributed to its micro/nanoscale hierarchical rough structures, as shown in Fig. 1f′. It is very clear from the image that the protuberances, which are like small peaks are spaced apart from each other. When wet with water, the peak shaped protuberances increase the CA between the water and scales, which gives superhydrophilic properties. Furthermore, these special hierarchical structures make it appear to be superaerophobic in aqueous media.[47] This discovery further developed the applications of fish scales. The biological phenomenon which was mentioned previously is highly significant and can be used to provide guidance to researchers and engineers to help them obtain excellent control of bubble behaviour and gas bubble wettability on a solid surface in a water medium.

3. Fundamental understanding of gas bubbles wettability in aqueous media

When a solid surface is immersed in a liquid, the behaviour of gas bubbles in aqueous media is largely similar to the behaviour of droplets on solid surfaces in air. The in air superhydrophilic surface generally shows superaerophobicity in aqueous

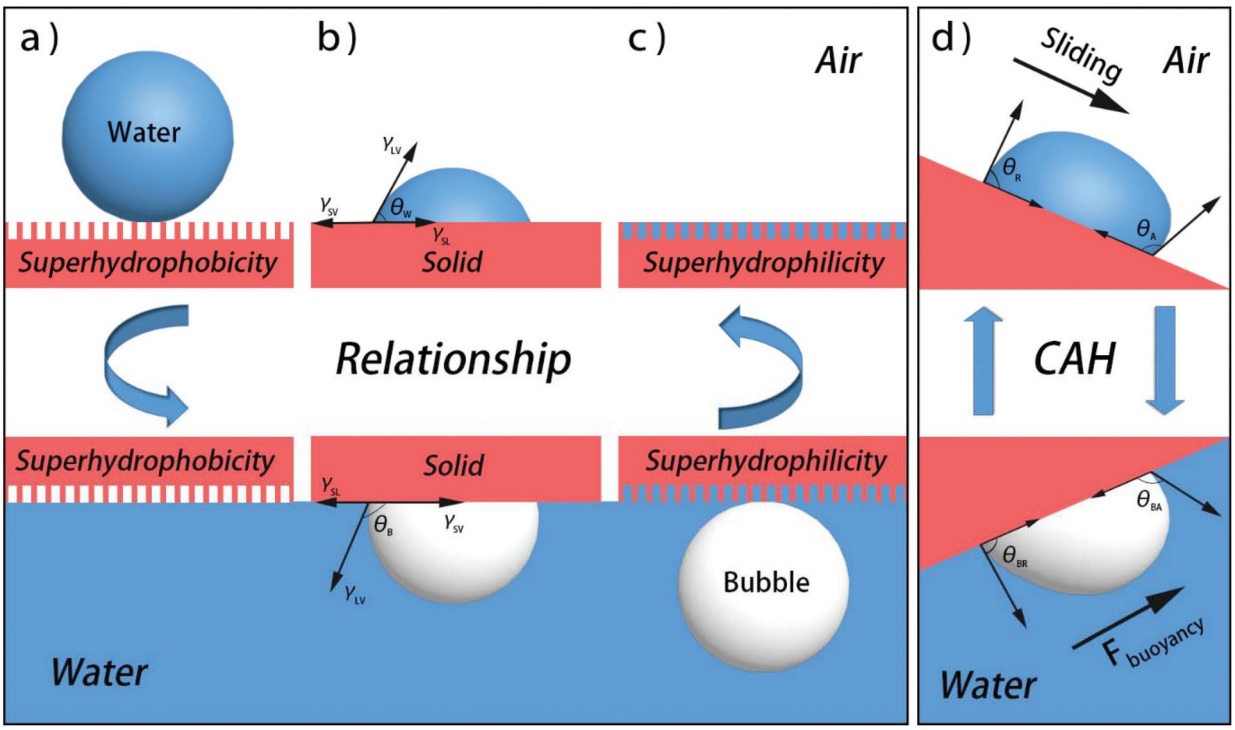

Fig. 2 Schematic diagrams showing the relationship between wettability of solids in air and water. (a),(b) and (c) show the comparison between wettability of drops in air and wettability of bubbles in water. (d) shows the similarity of CAH in different environments.

media and the in air superhydrophobic surface generally shows submerged superaerophilicity, as shown in Fig. 2a and c.[47] Thus, to better illustrate the wettability of gas bubbles, the two wetting conditions are compared together in the following section.

3.1 Contact angle and Young's equation in water

The wetting of solid surfaces by droplets is essentially a process of a gas–solid phase being replaced by a liquid–solid phase in air. The water molecules are spread out and as close as possible to the solid substrate. Some of the gas molecules are squeezed out by water molecules and the rest of them remain on the surface of the solid, keeping the three phase (solid/liquid/gas) balance. Therefore, the behaviour of bubbles is largely determined by the molecular forces between the three phases. Similarly, when a solid surface is immersed in an aqueous environment, the water molecules are in close proximity to the solid substrate, and the gas bubble molecules attempting to adhere to the substrate have to compete with the liquid film over the surface.[53] The competitive relationship between the gas phase and the liquid phase is the key factor determining the behaviour of underwater bubbles. Thus, wetting of an air bubble on an ideal solid surface immersed in water depends on the CA of a sessile droplet (θ_w) on the same substrate in air.[53] In order to measure the wettability of droplets, the concept of a CA is proposed. The CA of liquid droplets on solid surfaces is created by the surface tension of the interface between solid, liquid and gas. In an air environment, when the wetting process reaches equilibrium on an ideal solid surface, the interface tension forces of each phase satisfy Young's equation as follows:

$$\cos\theta_w = \frac{\gamma_{SV} - \gamma_{SL}}{\gamma_{LV}} \quad (1)$$

where γ_{SV}, γ_{SL}, and γ_{LV} represent the surface tension forces between solid-vapor, solid–liquid, and liquid–vapor, respectively. θ_w is the static WCA, as shown in Fig. 2b. Because of its generally similar nature, the concept of a bubble contact angle (BCA; θ_b) is also proposed:[54]

$$\theta_b = 180° - \theta_w \quad (2)$$

Subsequently, Young's equation can be rewritten in terms of θ_b as:

$$\cos(180° - \theta_b) = \frac{\gamma_{SV} - \gamma_{SL}}{\gamma_{LV}} \quad (3)$$

$$\cos\theta_b = \frac{\gamma_{SL} - \gamma_{SV}}{\gamma_{LV}} \quad (4)$$

Another way to derive this is based on the conservation of energy as follows:[55]

$$\delta_w = \gamma dA_{LV} + \gamma_{SL} dA_{SV} + \Delta P dV \quad (5)$$

where γ_{LV}, γ_{SL}, and γ_{SV} represent liquid–vapor, solid–liquid, and solid–vapor surface tensions, respectively. The dA_{LV}, dA_{SL}, dA_{SV}, are liquid–vapor, solid–liquid, and solid–vapor area changes, respectively, and ΔP is the Laplace pressure change

ΔP and dV is the volume change dV. If the conditions of $\delta_w = 0$, $\Delta V = 0$, $dA_{SL} = dA_{SV}$, and $dA_{LV}/dA_{SL} = \cos\theta$ for a semi-spherical shape are enforced with surface tension dominating over buoyancy, eqn (5) simplifies to the easily recognizable Young's equation of:

$$\gamma_{LV}\cos\theta = \gamma_{SV} - \gamma_{SL} \quad (6)$$

where, θ is the complement of θ_b. Eqn (6) can be written as:

$$\gamma_{LV}\cos(180^\circ - \theta_b) = \gamma_{SV} - \gamma_{SL} \quad (7)$$

$$\gamma_{LV}\cos\theta_b = \gamma_{SL} - \gamma_{SV} \quad (8)$$

eqn (8) further explains that gas bubble wettability in aqueous media can be approximately calculated as the complementary process of liquid wettability in air.

According to eqn (2) and (4), the value of the underwater BCA can be roughly calculated using the CA of droplets under the same conditions in air. Furthermore, the behaviour and existence of bubbles can be satisfactorily explained and predicted in different states. As mentioned previously, a superhydrophilic surface is superaerophobic in water. This is because of the complementary relationship between the BCA (θ_b) and the WCA (θ_w). When the WCA decreases, the bubble contact angle increases continuously, reaching superaerophobicity as shown in Fig. 2c.

It is worth noting that the relationship between the BCA (θ_b) and the WCA (θ_w) does not always satisfy the complementary angle. The most typical example of this is the phenomenon of the steady pinning effect of an air bubble on a rose petal. Rose petals are superhydrophobic surfaces, and the WCA is 152.4°, whereas its BCA reaches an amazing 126.9°.[25] Rose petals have the ability to capture bubbles and fix them on the surface because of their special hierarchical rough structures. These special structures endow the surfaces with a high contact angle hysteresis (CAH), which is the main cause of this phenomenon. CAH is described in detail in the following sections.

3.2 Bubble contact angle hysteresis (CAH_b)

The static CA of droplets on a smooth, solid, substrate surface have been shown to be inextricably linked to the CA of bubbles under water. When the droplet just rolls on the smooth surface because of gravity, a new concept CAH occurs. If the CA is measured while the volume of the drop is increasing, practically this is done just before the wetting line starts to advance, and it is called the advancing contact angle (ACA) θ_A. If afterwards the volume of the drop decreases and the CA is determined just before the wetting line is receding, the angle of this measurement is called the receding contact θ_R. The ACA is always larger than or equal to the RCA ($\theta_A < \theta_R$). The difference between the cosines of the two is called CAH as shown in Fig. 2d. For the wetting of the bubbles in water, the behavior of the bubbles on an ideal inclined solid surface is largely determined by buoyancy, because the bubbles are surrounded by water. Accordingly, bubbles also have the same properties on the solid surface in aqueous media, the bubble contact angle hysteresis (CAH_b).

A superhydrophobic surface has a low WCA (CAH, less than 5°) and also a high CA (more than 150°). Similarly, a superaerophobic interface defined as surfaces with a BCA of $\theta_b > 150^\circ$ and negligible hysteresis. However, surfaces with a BCA of $\theta_b \approx 0^\circ$and appreciable hysteresis are defined as superaerophilic interfaces.

3.3 Two states in water

Analogous to the wetting behavior of droplets on solid surfaces, there are two possible different states when a superhydrophobic or superhydrophilic surface is immersed in water: (1) like the Cassie–Baxter model in air, the rough solid surfaces are completely filled and covered by liquid so that the bubbles are fully lifted, showing a high BCA (θ_b) and negligible hysteresis as shown in Fig. 2c. (2) Because of the superhydrophobicity of solid surfaces, the gas bubbles are trapped and left behind to form a layer of air cushion, exhibiting the affinity of the gas and appreciable hysteresis as shown in Fig. 2a.[56] Importantly, it does not matter what type of state the bubbles are in underwater, they always follow the lowest energy principle and maintain the most stable state.

3.4 Contact force of bubbles

In an aqueous environment, the behavior of bubbles is mainly affected by adhesive force ($F_{adhesion}$). The value of this critical force is determined using the volume of bubbles and CAH_b. It can be calculated with the following formula:[57]

$$F_{adhesion} = kd\gamma_{LV}(\cos\theta_R - \cos\theta_A) \quad (9)$$

where γ_{LV}, k, d are the retentive force factor, surface tension of the liquid and diminished contact width, respectively. Undoubtedly, eqn (9) illustrates the fact that the wettability of bubbles is closely related to the contact width (d), which in turn affects the adhesive force. Furthermore, buoyancy as the main force affecting the contact width also plays a dominant role in surface tension.

The wetting of bubbles is essentially the process of replacing liquid molecules on the surface of a solid substrate with the molecules of a vapor. In this process, the vapor molecules are often covered by a thin layer of liquid film. Therefore, to better understand the wettability of bubbles, it is necessary to study the liquid film coated on the surface of bubbles. Fortunately, the bubble probe technique which is combination of surface force apparatus or atomic force microscopy (AFM) and reflection interference contrast microscopy (RICM) is found to measure the interaction contact force and spatial-temporal visualization of the thin-film drainage process.[56,58–62]

Reynolds lubrication theory and the augmented Young–Laplace equation are used to determine the interaction force and the spatiotemporal evolution of the confined thin water film.[59,63–66] In a liquid medium, the mechanism of the drainage dynamics of a thin liquid film in narrow gaps between

solids and bubbles is revealed using the Reynolds lubrication theory:

$$\frac{\partial h}{\partial t} = \frac{1}{12\mu}\frac{\partial}{\partial r}\left(rh^3\frac{\partial P}{\partial r}\right) \quad (10)$$

where μ is the viscosity of the liquid and r is the radial distance from the center of the film, h is the film thickness and t is time. However, when the liquid thin-film reaches a certain thickness, the influence comes mainly from hydrodynamic pressure, Laplace pressure and the disjoining force. Thus, the augmented Young-Laplace equation illustrates the relationship between them:

$$\frac{\gamma}{2r}\frac{\partial}{\partial r}\left(r\frac{\partial h}{\partial r}\right) = \frac{2\gamma}{R_0} - P - \Pi \quad (11)$$

where, R_0 is the radius of the bubble and γ is the surface tension of the liquid, P is the excess hydrodynamic pressure in the liquid film (between the air bubble and the solid) relative to the bulk liquid and Π is the disjoining pressure arising from van der Waals (vdW) interactions, electrical double layer (EDL) interactions, and hydrophobic interaction. Subsequently, integrating P and Π can be used to derive the overall interaction force $F(t)$ of the air bubble on the solid surface:

$$F(t) = 2\pi\int_0^{\infty}[P(r,t) + \Pi(h(r,t))]r\mathrm{d}r \quad (12)$$

Zeng and co-workers have made good progress in this respect.[67–69] They measured forces and spatiotemporal evolution of thin water films between an air bubble and mica surfaces of different hydrophobicity in a comprehensive and multidirectional way. The interaction forces were measured using AFM by driving a cantilever anchored air bubble towards the mica surface in 500 mM of sodium chloride (NaCl) solution at a velocity of 1 μm s^{-1}. The fringe patterns that arose from interference between light reflected from the air/water interface of the bubble and the mica/water surface were obtained using RICM and analysed using eqn (10) and (11) as shown in Fig. 3a.[61]

For hydrophilic mica surfaces, it is worth knowing that a high concentration of NaCl made the contribution ($\Pi_{EDL}(h(r, t))$) of the EDL interaction between the bubble and the mica surfaces to the whole disjoining pressure ($\Pi(h(r,t))$) insignifi-

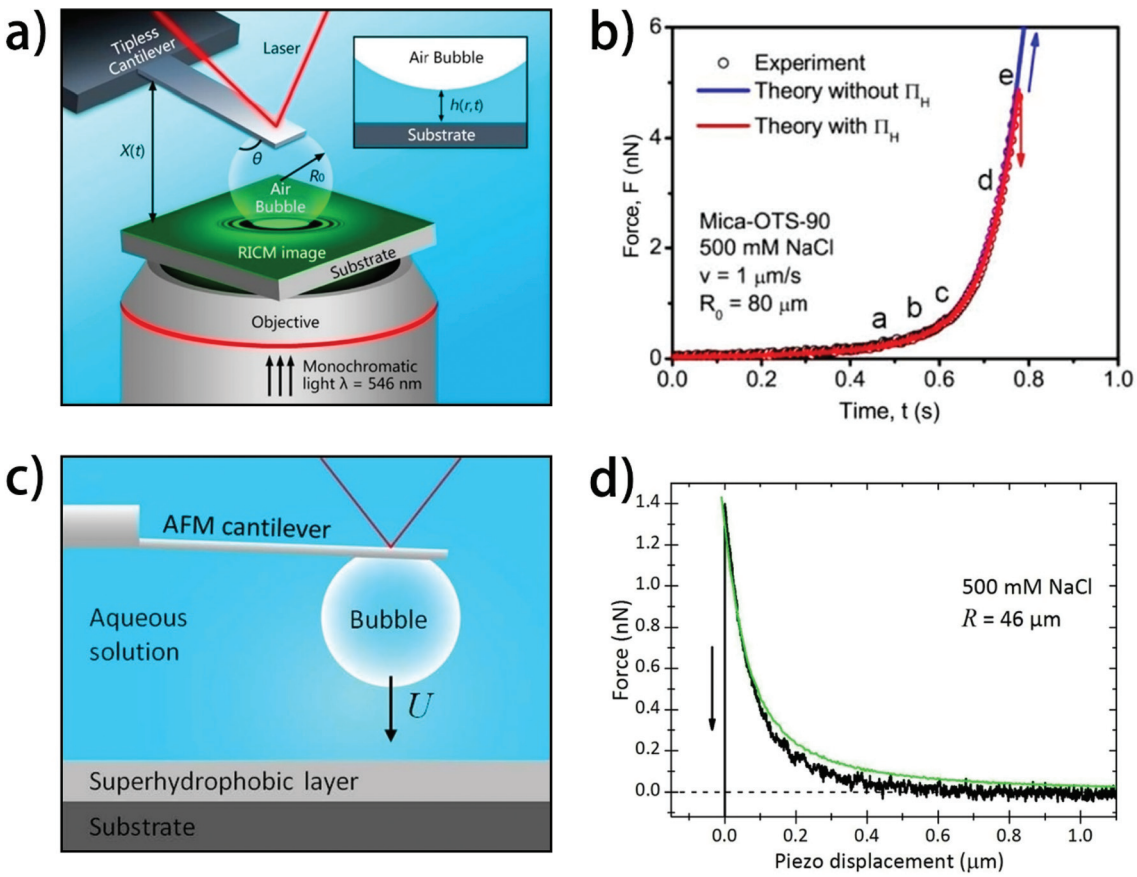

Fig. 3 Measuring the interaction forces between an air bubble and surfaces of different hydrophobicity by using AFM in combination with RICM. (a) and (c) The device for studying bubble wettability which integrate AFM and RICM. (b) The interaction force of bubble on the mica surfaces changing with time, on which the "jump in" phenomenon can be clearly seen. (d) The interaction force of bubble on the soot-templated superhydrophobic surfaces changing with piezo-displacement. (a) and (b) reproduced from ref. 61 with permission from *ACS Nano*. Copyright 2015. (b) and (c) Reproduced from ref. 56 with permission from *Langmuir*. Copyright 2015.

cant. Thus, the main disjoining pressure is derived entirely from vdW interactions. Furthermore, based on the Lifshitz theory of vdW force, the vdW interaction of bubbles and mica surfaces is repulsive which maintained a thin water film between the air bubble and the hydrophilic mica surfaces.[61]

For hydrophobic mica surfaces, a "jump-in" phenomenon was observed when the bubble was close to the hydrophobic surfaces as shown in Fig. 3b. According to the classical wetting model, the sudden decrease of the force caused the thin water film under the bubble to be completely removed and the bubble contacted the gas layers on the hydrophobic surfaces.[61] When the negative disjoining pressure just exceeds the Laplace pressure of the bubble, the bubble attaches to the surface, as shown in eqn (11).

Shi *et al.* continued the research and studied the interaction between air bubbles and superhydrophobic surfaces in almost the same way as shown in Fig. 3e.[56] They found that once the EDL force and a hydrodynamic repulsion were overcome, bubbles jumped onto the surface and fully merged with the entrapped air. Furthermore, the same "jump in" behavior was observed on the soot templated surfaces, which indicated that the superhydrophobic surface is superaerophilic under water as shown in Fig. 3f. At the same time, Cao *et al.* also studied and discussed this problem.[70] They argue that the two wetting states could not be completely equivalent, and they also designed experiments to use superhydrophobic surface defects to achieve controlled directional bubble transport in aqueous media. These theories and experiments opened up a new field in the research and application of underwater bubble wettability.

To better illustrate the wettability of gas bubbles, the difference and similarity between the wettability of underwater bubbles and the wettability of water drops in the air are summarized in Table 1.

4. Functions and applications

With further study of bubble wettability, various theories and fabrication methods have been improved. At the same time, superaerophobicity and superaerophobicity surfaces have been shown to have special applications in many other fields. For example, superaerophilic electrodes for GCRs, superaerophobic electrodes for GERs, gas-bubble transport on interfaces with superwettability of bubbles and so on.

4.1 Superaerophilic electrodes for GCRs

The GCRs including the oxygen reduction reaction (ORR) is a crucial step for determining the performances of various power storage and release equipment in electrochemical reactions involving gases. One of the main limiting factors is the inadequate reactive gases.[71] It is very difficult, and uneconomical, to enhance their performance by improving the catalyst. In fact, the solubility of gas is extremely low and its diffusion rate is very low in an aqueous electrolyte. The shortage of gas in an ORR on an electrode often limits its further reaction rate. Not getting an oxygen (O_2) supplement in time makes the next reaction impossible. Thus, to remove this dilemma a desirable architecture was designed to facilitate electron transport from the current collector to the catalyst layer and provide an unobstructed gas diffusion pathway to continually supply enough gas reactant to the reactive catalytic sites. The novel structures which use the new three-phase contact point (TPCP) instead of the original two-phase contact allow gas to participate more easily in the reaction. Because of its superaerophilic properties, a stable gas layer is formed on the electrode surfaces instead of being wetted so that a lot of TPCPs greatly enhanced the gas diffusion rate and it also guarantees the electron transmission efficiency.

Sun and co-workers achieved this concept by fabricating porous cobalt incorporated nitrogen-doped carbon nanotube (CoNCNT) arrays on carbon-fibre paper (CFP) as shown in Fig. 4a.[40] They used direct natural growth to ensure the compactness and high conductivity of the nanoarrays, and modified the highly roughened surfaces using poly(tetrafluoroethylene) (PTFE) to give them superaerophilic properties with a stable oxygen gas layer under aqueous media. Because of the unique architecture, the TPCP, the electron transmission efficiency and enough gas reactant was kept at a relatively balanced level, it gave an excellent ORR performance in both base and acid media.

Similarly, Feng and co-workers immobilized glucose oxidase (GO_x) on platinum (Pt) catalyst modified conducting superaerophilic carbon fiber mesh, which is used as an electrochemical STP-biosensor as shown in Fig. 4b.[72] A stable and adequate layer of oxygen was formed on the surfaces to solve the problem of insufficient oxygen supply when the superaerophilic multi-layer micro/nano structure electrode was immersed in the analyte solution. This ingenious design replaced two-phase contact with TPCP, in which oxygen

Table 1 A comparison between the wettability of underwater bubbles and the wettability of the water drops in the air

	Contact angle	Young's equation	Contact angle hysteresis	Wetting states
The wettability of gas bubbles in aqueous media	$\theta_b = 180° - \theta_w$	$\cos\theta_b = \frac{\gamma_{SL} - \gamma_{SV}}{\gamma_{LV}}$	$CAH_b = \cos R_b - \cos A_b$	Superaerophobic Aerophobic Aerophilic Superaerophilic
The wettability of the drops in The air	θ_w	$\cos\theta_w = \frac{\gamma_{SV} - \gamma_{SL}}{\gamma_{LV}}$	$CAH_w = \cos R_w - \cos A_w$	Superhydrophobic Hydrophobic Hydrophilic Superhydrophilic

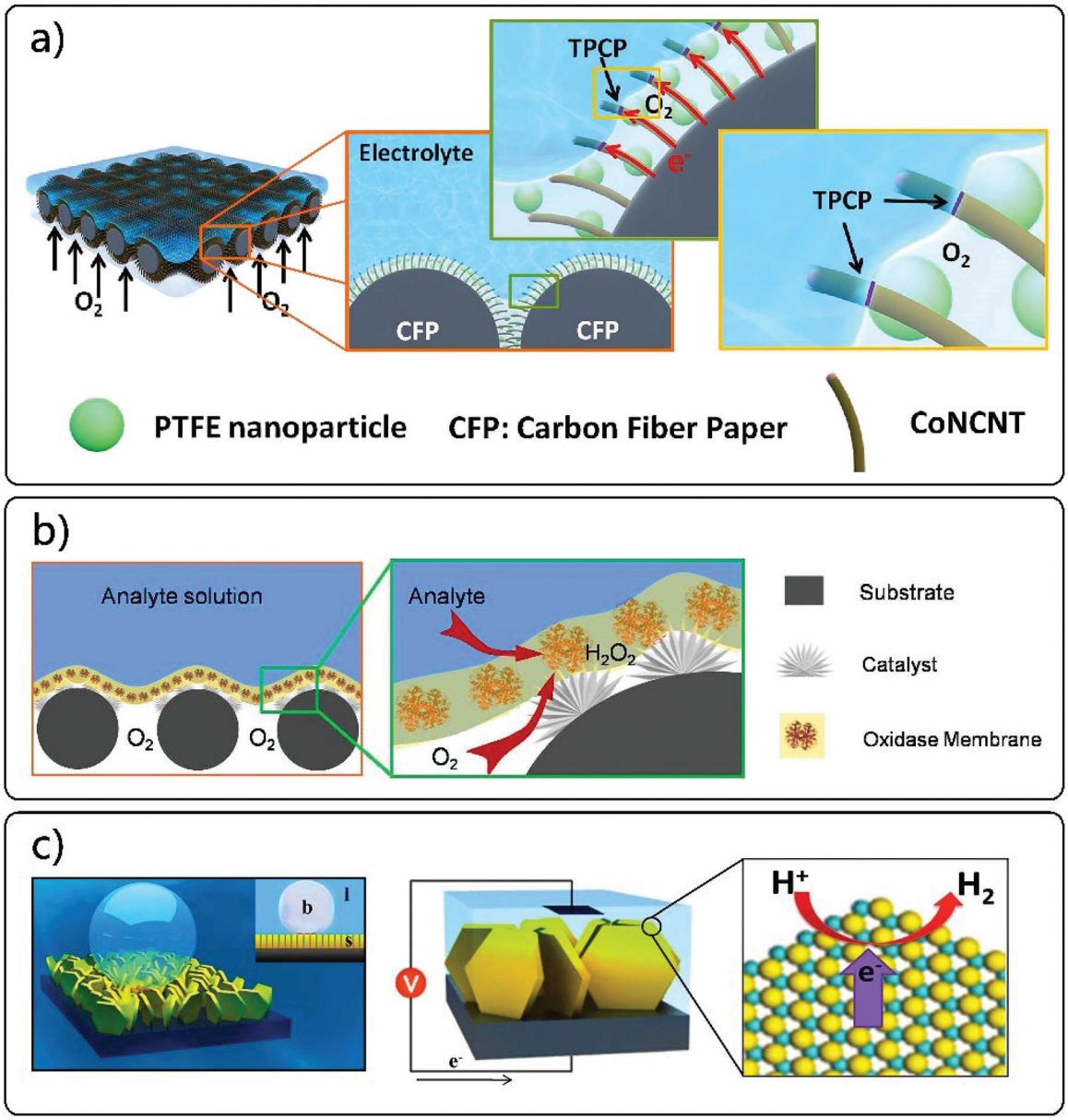

Fig. 4 Superaerophilic and superaerophobic electrodes used in GARs and GERs. (a) The superaerophilic electrode is covered by directly growing CoNCNTs on CFP associated with subsequent PTFE-modification. The intimate connection of the catalyst to the substrate offers an accelerated electron-transport process, and the highly porous structure provides abundant nanoscale TPCP for ORR. Both electron-transport and oxygen-diffusion processes are accelerated, leading to a superior ORR performance. Reproduced from ref. 40 with permission from *Advanced Materials*. Copyright 2016. (b) It is fabricated by superaerophilic electrode, which is constructed using Pt-catalyst-modified carbon-fibre mesh. Reproduced from ref. 72 with permission from *Advanced Materials*. Copyright 2016. (c) Superaerophobic electrode interface constructed by vertically aligned MoS_2 nanoplatelets (typically 200 nm in size and less than 5 nm thick). Schematic of nanostructured MoS_2 electrode. The active Mo edge for HER is marked in the magnified image of the crystal structure. The rapid removal of small gas bubbles can provide a constant working area for the HER reaction. Blue sphere, Mo; yellow sphere, S. Reproduced from ref. 27 with permission from *Advanced Materials*. Copyright 2014.

diffused directly from the air phase to the oxidase active sites. The successful manufacture of the STP-biosensor indicates that the superhydrophilic surfaces provide a unique way to solve the gas shortage problem in many reaction systems. In addition, Liu *et al.* highly boosted ORR activity by tuning the underwater wetting state of the superaerophilic electrode, which achieved satisfactory results and further developed the application of superaerophilic surfaces in electrodes.[37] A summary of these electrodes is given in Table 2.

4.2 Superaerophobic electrodes for GERs

The GERs generally refers to the process of producing a gas phase on electrodes in a liquid phase reactant in an electrochemical reaction. For example, water splitting generates a

Table 2 The application of electrodes for different electrochemical reactions and examples

Electrodes wettability	Reaction types	Application	Examples
Superaerophilic electrodes	GCRs	Forming gas layer to build more TPCPs to provide a stable and sufficient gas volume to participate in the reaction.	Superaerophilic carbon nanotube array electrode,[40] oxygen-rich enzyme biosensor,[72] superaerophilic pillar structure substrate electrode,[37] a novel method for producing gas diffusion layers with patterned wettability,[73] a vapor phase–polymerized PEDOT Electrode[74]
Superaerophobic electrodes	HER	Preventing gas adhesion from stacking electrode surfaces	MoS_2 thin film nanosheet arrays,[27] pine-shaped Pt nanoarray electrode,[75] Pt nanosheet boron-doped diamond electrode,[76] Ni_2P nanoarray electrode,[77] SiO_2–polypyrrole hybrid nanotubes supported on carbon fibers[78]
	OER	Reduce the size of the bubble	Cu_3P microsheets,[79] NiFe-LDH nanoplates,[80] plasma-engraved Co_3O_4 Nanosheets,[81] Ni_3S_2 nanosheet arrays,[82] $Zn_xCo_{3-x}O_4$ nanoarrays[83]
	HzOR	Increase the escape velocity of the bubble	3D nanostructured Cu nanoarrays,[84] superaerophobic graphene nano-hills,[85] single-crystalline ultrathin nickel nanosheet array[86]
	CIER		RuO_2@TiO_2 nanosheet array[36]

hydrogen (H_2) and O_2 gas phase on the electrodes in the liquid phase. In GERs, a three-phase interface consisting of gas phase, liquid phase and solid phase is formed on the electrode surfaces, and the gas phase usually separates and escapes directly. However, in some industrial reactions a large number of bubbles often accumulate on the electrode surfaces because of the excessive reaction rate, which blocks the generation of the reaction and reduces the reaction rate. Thus, superaerophobic electrodes are widely used in GERs including the hydrogen evolution reaction (HER), the oxygen evolution reaction (OER), the hydrazine oxidation reaction (HzOR), the and chlorine evolution reaction (ClER), to solve this problem. Lu and co-workers fabricated a molybdenum disulfide (MoS_2) nanostructured film, which contained vertically aligned MoS_2 nanoplatelets (typically 200 nm in size and less than 5 nm in thickness), as superaerophobic electrodes used for HER as shown in Fig. 4c.[28] Because of the low adhesion of the bubbles, superaerophobic electrodes prevent gas bubbles from accumulating on the electrode surfaces to form a gas layer that isolates the reactants. Thus, the bubbles detach from the electrode surfaces while they are a small size and the two-phase contact between the liquid phase and the solid phase is constantly sustained, which achieves an efficient HER. Furthermore, in view of the various GERs, more superaerophobic electrodes with different materials, different preparation methods and different structures were fabricated. The application of electrodes for different electrochemical reactions and examples are given in Table 2.

4.3 Air bubble transport on interfaces with superwettability of bubbles

The wettability of bubbles is not only widely used in electrochemical reactions, but also plays an important role in the transport of gases. According to the "bubble burst effect" on the lotus leaf, when the superaerophilic interface is immersed in a water environment, the bubbles burst and spread rapidly on its surface to form a gas layer. This special property can be used for the absorption and transport of gases. Inspired by this, Su and co-workers constructed a novel underwater superaerophilic sponge for selective collection, stable storage and continuous transport of gas.[87] The sponge modified with a porous structure and superaerophilic poly(urethane) (PU) has a certain selectivity to gas under water as shown in Fig. 5a. The bubbles quickly burst and spread on its surfaces, and are collected continuously by direct transport. On the contrary, water is blocked by superaerophilic sponge.

Subsequently, they improved the superaerophilic sponge to successfully absorb methane gas, which had great significance for reducing greenhouse gases and reducing the greenhouse effect as shown in Fig. 5a.

In nature, many organisms have the ability to capture and transport water directly from the environment, using specialized materials such as spider silk and cactus spines.[90,91] Researchers discovered that this ability is because of the unique surfaces of the multilevel micro/nano structures, which yield to the gradient of the Laplace pressure and surface free energy to serve as the cooperative driving forces to transport water droplets directionally.[92–94] Based on this behaviour, Wang and co-workers manufactured a superaerophilic copper wire with a type of 3D gradient porous interconnected network.[95] Because of the combination of the prepared unique surfaces and a simple to control electrochemical method, the copper wires can maintain a perfectly constant gas layer in an aqueous medium. At the same time, gas bubbles can be continuously and directionally transported through the film on the surfaces by the difference of the Laplace pressure.

Ultimately, Li and co-workers fabricated a helical superaerophilic copper wire and found that the bubble tends to stay on the summit of the helix structure and moves along with the helix rotation in an aqueous environment.[89] The buoyancy force of the bubbles in water and the adhesion force of the bubbles to the copper wire are simultaneous. The direction of the adhesion force is always perpendicular to the surface of the copper wires, but the direction of the buoyancy force is always

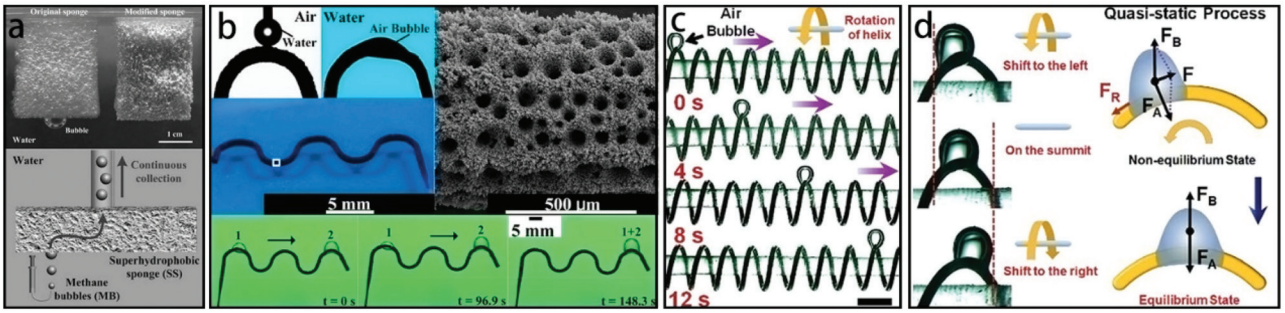

Fig. 5 (a) The sponge modified by PU; continuous collection and transport bubbles in water. Reproduced from ref. 87 with permission from *Langmuir*. Copyright 2010. (b) The microstructure of the superhydrophilic surface and the transport of bubbles on its surface. Reproduced from ref. 88 with permission from *Angewandte Chemie*. Copyright 2017. (c) and (d) The structure and transport of bubbles schematic diagram of a helical superaerophilic copper wire. Reproduced from ref. 89 with permission from *Journal of Materials Chemistry A*. Copyright 2016.

vertical as shown in Fig. 5d. When the angle of the copper wire changes, the adhesive force of the bubble can be offset by the component of the buoyancy force, while the remaining component of the buoyancy force drives the bubble to the top of the helix, and at this point the buoyancy force and the adhesion force are balanced. Therefore, the copper wire is continuously rotated in one direction, while the bubble will always move afterwards as shown in Fig. 5c. In this way, the direction and rate of the bubbles' transport can be precisely controlled by adjusting the length, direction and rotation speed of the copper wire. Based on the multiple control of the bubble, more and more superaerophilic surfaces are produced. However, the most reliable and effective way to manipulate bubbles occurs on the interfaces with simple shapes, *i.e.*, cylindrical and cone shapes in the water medium. Wang and co-workers carried out further discussion and research on this question with a type of three-dimensional (3D) gradient porous network which was constructed on copper wire interfaces, with rectangle, wave, and helix shapes as shown in Fig. 5b.[88] It was eventually found that the average velocity of the bubble was related to the shape of the copper wire, and the small gas bubble spontaneously and directionally moves to the larger bubbles. Based on these research theories, more and more wettabilities of bubble surfaces have been designed to control bubbles in aqueous environments.[96–99]

Yu and co-workers illustrated that on the interfaces with a gradient curvature, the bubbles exhibit different behaviours on the interface with different bubble wettabilities, which include aerophilicity, superaerophilicity, aerophobicity and superaerophobicity.[100] When a bubble encounters a superaerophobic or aerophobic interface, the bubble bounces away because of small adhesive forces, as shown in Fig. 6a and b. This phenomenon indicates that the superaerophobic or aerophobic cones cannot capture or transport bubbles. Conversely, an aerophilic cone can easily capture bubbles, but can only transport bubbles for a short distance as shown in Fig. 6c. In fact, this transient transport process is achieved through continuous aggregation of bubbles, but as buoyancy continues to increase, the bubbles will eventually escape into the water. The Laplacian pressure gradient can only be produced on the other

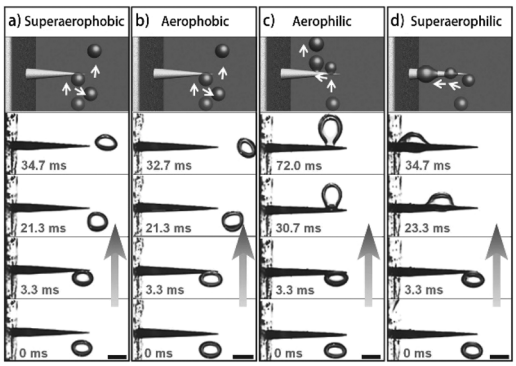

Fig. 6 On the interfaces with gradient curvature, the bubbles exhibit different behavior on the interface with different bubble wettabilities. (a) and (b) The bubbles encounter a superaerophobic or aerophobic cone, and the bubble bounces away. (c) An aerophilic cone can easily capture bubbles, but can only transport bubbles for a short distance. (d) A superaerophilic cone can easily capture bubbles and transport bubbles for a long distance. Reproduced from ref. 100 with permission from *Advanced Functional Materials*. Copyright 2016.

side of the bubble by introducing bubbles into the superaerophilic interface with gradient curvature. Only in the case of a Laplacian pressure gradient can the bubbles be continuously and steadily transported directly to the root of the cones regardless of the direction as shown in Fig. 6d. In addition, this cone-shaped superaerophilic surface can also continuously collect and directionally transport carbon dioxide (CO_2) microbubbles in CO_2 supersaturated solutions[101] or H_2 microbubbles for HER,[102] and control the size of the bubbles.[105]

In the superwettability of surfaces, there are two different wettability interfaces called Janus. In the same way, the manipulation of bubbles could be achieved by using bubbles with different wettabilities on the Janus interfaces. A superhydrophobic/hydrophilic cooperative Janus mesh has very interesting properties. In an aqueous environment, when the superaerophilic side is placed on top, bubbles under the membrane form a larger bubble through its mesh.[103,104] When the superaerophobicity side is facing upwards, bubbles are blocked by the membrane and form a large air bubble. This kind of intel-

ligent Janus membrane with one-way air bubble transport can realize intelligent control of air bubbles just like the "diode" of an underwater air bubble, which has a potential application in the development and design of functional devices.

Yang and co-workers reported a superaerophobic-hydrophobic Janus membrane with asymmetric wettability for fine bubble aeration.[103] The hydrophobic side prevents water from penetrating through the membrane holes and draws in the gas to reduce the pressure, while the superaerophobic side, which is achieved by adjusting the surface wettability and hierarchical structures, makes the bubbles detach rapidly and decreases the volume of the bubbles. Therefore, the goals of fine bubble aeration are realized.

5. Conclusions and prospects for the future

In this review, the recent progress in wettability of bubbles in aqueous media has been briefly summarized, including natural species with superwettability of bubbles, theoretical background, functions and applications, using an appropriate classification. Subsequently, issues and challenges were discussed objectively and some prospects for the future development of the bubble superwettability interfaces are presented next:

• Nature is a treasure trove for scientific research, in which many biological surfaces exhibit marvellous characteristics. Numerous natural interface structures remain to be explored and developed as more is learned from nature.

• At present, the theories of bubble wettability remain to complement and improve. For example, a more scientific and concise definition of bubble superwettability (superaerophobic and superaerophilic) needs to be considered. Whether the superaerophilicity in water can be equated with the superhydrophobicity in air, a complete and systematic theory for the relationship between the wettability of bubbles underwater and the wettability of droplets in the air remains to be determined. Although AFM in combination with RICM can be used to measure the interaction forces between an air bubble and surfaces of different hydrophobicity, the operation is complicated and there are many other limiting factors for it to be used in practical applications. Thus, a new method for measuring bubble wettability which is simpler and more comprehensive needs to be developed.

• Even though various bionic and artificial interfaces for bubble superwettability have been created, this field is still in its infancy. As is known, the superaerophobic and superaerophilic surfaces need to be immersed in the water environment for them to show their special properties. However, only in Cassie–Baxter models, can the interface have the characteristics of superaerophilicity. Thus, the longevity of artificial interfaces is a serious problem. A long-life and durable interfacial material urgently needs to be designed and fabricated, which can maintain wettability under water for a long time.

• By simulating the macroscopic behavior of some organisms, useful artificial interfaces which have micro/nanohierarchical structures and chemical compositions can be manufactured to manipulate the gas-bubbles superwettability. The effective and available manipulation of gas bubble superwettability is a novel idea and a method to solve various practical problems in aspects, *e.g.*, superaerophobic electrodes for GERs, superaerophilic electrodes for GCRs, superaerophilic interfaces for directional collection and transportation of gas bubbles, and so on. However, problems and challenges still exist. In practical applications, the complex environment including different physical and chemical conditions, the flow rate of the solution, changes in buoyancy and adhesion, pH value and immersion depth, and so on, will have an unpredictable impact on surfaces of bubble wettability. Thus, more attempts should be expended to prepare the interfaces in different media, in different ways and using different structures.

In summary, the field of bubble wettability research is still in the early stages. The ultimate goal of artificial superaerophobic/superaerophilic surfaces is the perfect combination of preparation methods, structural and functional characteristics and practical applications. Therefore, enormous efforts are required to achieve this goal.

Conflicts of interest

There are no conflicts to declare.

Acknowledgements

This work is supported by the National Nature Science Foundation of China (No 51522510, 51675513 and 51735013).

Notes and references

1 C. M. Yu, X. B. Zhu, M. Y. Cao, C. L. Yu, K. Li and L. Jiang, *J. Mater. Chem. A*, 2016, **4**, 16865–16870.
2 S. H. Huynh, A. A. A. Zahidi, M. Muradoglu, B. H. P. Cheong and T. W. Ng, *Langmuir*, 2015, **31**, 6695–6703.
3 X. F. Gao and L. Jiang, *Nature*, 2004, **432**, 36–36.
4 A. R. Parker and C. R. Lawrence, *Nature*, 2001, **414**, 33–34.
5 G. S. Watson, B. W. Cribb and J. A. Watson, *ACS Nano*, 2010, **4**, 129–136.
6 R. S. Seymour and S. K. Hetz, *J. Exp. Biol.*, 2011, **214**, 2175–2181.
7 H. W. Levi, *Evolution*, 1967, **21**, 571–583.
8 B. Messner and J. Adis, *Dtsch. Entomol. Z.*, 1995, **42**, 453–459.
9 W. Barthlott and C. Neinhuis, *Planta*, 1997, **202**, 1–8.
10 L. Feng, S. H. Li, Y. S. Li, H. J. Li, L. J. Zhang, J. Zhai, Y. L. Song, B. Q. Liu, L. Jiang and D. B. Zhu, *Adv. Mater.*, 2002, **14**, 1857–1860.

11 D. Oner and T. J. McCarthy, *Langmuir*, 2000, **16**, 7777–7782.
12 H. J. Tsai and Y. L. Lee, *Langmuir*, 2007, **23**, 12687–12692.
13 H. Gau, S. Herminghaus, P. Lenz and R. Lipowsky, *Science*, 1999, **283**, 46–49.
14 A. Tuteja, W. J. Choi, G. H. McKinley, R. E. Cohen and M. F. Rubner, *MRS Bull.*, 2008, **33**, 752–758.
15 T. Liu, Y. S. Yin, S. G. Chen, X. T. Chang and S. Cheng, *Electrochim. Acta*, 2007, **52**, 3709–3713.
16 S. A. Kulkami, S. B. Ogale and K. P. Vijayamohanan, *J. Colloid Interface Sci.*, 2008, **318**, 372–379.
17 D. Quere, *Rep. Prog. Phys.*, 2005, **68**, 2495–2532.
18 K. Satoh and H. Nakazumi, *J. Sol-Gel Sci. Technol.*, 2003, **27**, 327–332.
19 T. Kako, A. Nakajima, H. Irie, Z. Kato, K. Uematsu, T. Watanabe and K. Hashimoto, *J. Mater. Sci.*, 2004, **39**, 547–555.
20 T. L. Sun, L. Feng, X. F. Gao and L. Jiang, *Acc. Chem. Res.*, 2005, **38**, 644–652.
21 X. B. Zhang, J. Zhao, Q. Zhu, N. Chen, M. W. Zhang and Q. M. Pan, *ACS Appl. Mater. Interfaces*, 2011, **3**, 2630–2636.
22 X.-M. Li, D. Reinhoudt and M. Crego-Calama, *Chem. Soc. Rev.*, 2007, **36**, 1350–1368.
23 B. Wang, Y. B. Zhang, L. Shi, J. Li and Z. G. Guo, *J. Mater. Chem.*, 2012, **22**, 20112–20127.
24 D. Bonn, J. Eggers, J. Indekeu, J. Meunier and E. Rolley, *Rev. Mod. Phys.*, 2009, **81**, 739–805.
25 N. Ishida, M. Sakamoto, M. Miyahara and K. Higashitani, *J. Colloid Interface Sci.*, 2002, **253**, 112–116.
26 H. de Maleprade, C. Clanet and D. Quere, *Phys. Rev. Lett.*, 2016, **117**, 094501.
27 J. M. Wang, Q. L. Yang, M. C. Wang, C. Wang and L. Jiang, *Soft Matter*, 2012, **8**, 2261–2266.
28 C. M. Yu, P. P. Zhang, J. M. Wang and L. Jiang, *Adv. Mater.*, 2017, **29**, 1703053.
29 Z. Y. Lu, W. Zhu, X. Y. Yu, H. C. Zhang, Y. J. Li, X. M. Sun, X. W. Wang, H. Wang, J. M. Wang, J. Luo, X. D. Lei and L. Jiang, *Adv. Mater.*, 2014, **26**, 2683–2687.
30 Md. S. K. AlamSarkar, S. W. Donne and G. M. Evans, *Adv. Powder Technol.*, 2010, **21**, 412–418.
31 H. Odegaard, *Water Sci. Technol.*, 2001, **43**, 75–81.
32 M. S. Siddiqui, G. L. Amy and B. D. Murphy, *Water Res.*, 1997, **31**, 3098–3106.
33 U. von Gunten, *Water Res.*, 2003, **37**, 1443–1467.
34 T. A. Ternes, M. Meisenheimer, D. McDowell, F. Sacher, H. J. Brauch, B. H. Gulde, G. Preuss, U. Wilme and N. Z. Seibert, *Environ. Sci. Technol.*, 2002, **36**, 3855–3863.
35 B. Bhushan and Y. C. Jung, *Prog. Mater. Sci.*, 2011, **56**, 1–108.
36 S. K. Mazloomi and N. Sulaiman, *Renewable Sustainable Energy Rev.*, 2012, **16**, 4257–4263.
37 M. S. Faber, R. Dziedzic, M. A. Lukowski, N. S. Kaiser, Q. Ding and S. Jin, *J. Am. Chem. Soc.*, 2014, **136**, 10053–10061.
38 P. W. Wang, T. Hayashi, Q. A. Meng, Q. B. Wang, H. Liu, K. Hashimoto and L. Jiang, *Small*, 2017, **13**, 1601250.
39 J. Zhang, X. Sheng, X. Q. Cheng, L. P. Chen, J. Jin and X. J. Feng, *Nanoscale*, 2017, **9**, 87–90.
40 Q. N. Wang, H. Dong and H. B. Yu, *J. Power Sources*, 2014, **271**, 278–284.
41 R. L. Machunda, J. Lee and J. Lee, *Surf. Interface Anal.*, 2010, **42**, 564–567.
42 Z. Y. Lu, W. W. Xu, J. Ma, Y. J. Li, X. M. Sun and L. Jiang, *Adv. Mater.*, 2016, **28**, 7155–7161.
43 J. M. Wang, Y. M. Zheng, F. Q. Nie, J. Zhai and L. Jiang, *Langmuir*, 2009, **25**, 14129–14134.
44 Z. Cerman, B. F. Striffler and W. Barthlott, *Functional Surfaces in Biology*, Springer Netherlands, Dordrecht, 2009, 97–111.
45 Y. M. Park, M. Gang, Y. H. Seo and B. H. Kim, *Thin Solid Films*, 2011, **520**, 362–367.
46 D. Neumann and D. Woermann, *Springerplus*, 2013, **2**, 694.
47 R. S. Seymour and P. G. D. Matthews, *J. Exp. Biol.*, 2013, **216**, 164–170.
48 A. Balmert, H. F. Bohn, P. Ditsche-Kuru and W. Barthlott, *J. Morphol.*, 2011, **272**, 442–451.
49 J. L. Yong, F. Chen, Y. Fang, J. L. Huo, Q. Yang, J. Z. Zhang, H. Bian and X. Hou, *ACS Appl. Mater. Interfaces*, 2017, **9**, 39863–39871.
50 W. Barthlott, T. Schimmel, S. Wiersch, K. Koch, M. Brede, M. Barczewski, S. Walheim, A. Weis, A. Kaltenmaier, A. Leder and H. F. Bohn, *Adv. Mater.*, 2010, **22**, 2325–2328.
51 L. Feng, Y. A. Zhang, J. M. Xi, Y. Zhu, N. Wang, F. Xia and L. Jiang, *Langmuir*, 2008, **24**, 4114–4119.
52 M. R. Flynn and J. W. M. Bush, *J. Fluid Mech.*, 2008, **608**, 275–296.
53 C. Neinhuis and W. Barthlott, *Ann. Bot.*, 1997, **79**, 667–677.
54 M. J. Liu, S. T. Wang, Z. X. Wei, Y. L. Song and L. Jiang, *Adv. Mater.*, 2009, **21**, 665–669.
55 P. C. Zhang, S. S. Wang, S. T. Wang and L. Jiang, *Small*, 2015, **11**, 1939–1946.
56 W. Y. L. Ling, G. Lu and T. W. Ng, *Langmuir*, 2011, **27**, 3233–3237.
57 C. Shi, X. Cui, X. R. Zhang, P. Tchoukov, Q. X. Liu, N. Encinas, M. Paven, F. Geyer, D. Vollmer, Z. H. Xu, H. J. Butt and H. B. Zeng, *Langmuir*, 2015, **31**, 7317–7327.
58 J. E. George, S. Chidangil and S. D. George, *Adv. Mater. Interfaces*, 2017, **4**, 1601088.
59 E. E. Meyer, K. J. Rosenberg and J. Israelachvili, *Proc. Natl. Acad. Sci. U. S. A.*, 2006, **103**, 15739–15746.
60 M. Krasowska, R. Krastev, M. Rogalski and K. Malysa, *Langmuir*, 2007, **23**, 549–557.
61 C. Shi, D. Y. C. Chan, Q. X. Liu and H. B. Zeng, *J. Phys. Chem. C*, 2014, **118**, 25000–25008.
62 C. Shi, X. Cui, L. Xie, Q. X. Liu, D. Y. C. Chan, J. N. Israelachvili and H. B. Zeng, *ACS Nano*, 2015, **9**, 95–104.
63 M. H. W. Hendrix, R. Manica, E. Klaseboer, D. Y. C. Chan and C. D. Ohl, *Phys. Rev. Lett.*, 2012, **108**, 247803.
64 R. Manica, E. Klaseboer and D. Y. C. Chan, *Soft Matter*, 2016, **12**, 3271–3282.

65 V. V. Yaminsky, S. Ohnishi, E. A. Vogler and R. G. Horn, *Langmuir*, 2010, **26**, 8061–8074.
66 H. J. An, G. M. Liu and V. S. J. Craig, *Adv. Colloid Interface Sci.*, 2015, **222**, 9–17.
67 L. Pan and R. H. Yoon, *Miner. Eng.*, 2016, **98**, 240–250.
68 X. Cui, C. Shi, L. Xie, J. Liu and H. B. Zeng, *Langmuir*, 2016, **32**, 11236–11244.
69 L. Xie, J. Y. Wang, D. W. Yuan, C. Shi, X. Cui, H. Zhang, Q. Liu, Q. X. Liu and H. B. Zeng, *Langmuir*, 2017, **33**, 2353–2361.
70 L. Xie, C. Shi, X. Cui, J. Huang, J. Y. Wang, Q. Liu and H. B. Zeng, *Langmuir*, 2018, **34**, 729–738.
71 M. Y. Cao, Z. Li, H. Y. Ma, H. Geng, C. M. Yu and L. Jiang, *ACS Appl. Mater. Interfaces*, 2018, **10**, 20995–21000.
72 J. L. Zhang, M. B. Vukmirovic, K. Sasaki, A. U. Nilekar, M. Mavrikakis and R. R. Adzic, *J. Am. Chem. Soc.*, 2005, **127**, 12480–12481.
73 Y. J. Lei, R. Z. Sun, X. C. Zhang, X. J. Feng and L. Jiang, *Adv. Mater.*, 2016, **28**, 1477–1481.
74 A. Forner-Cuenca, J. Biesdorf, L. Gubler, P. M. Kristiansen, T. J. Schmidt and P. Boillat, *Adv. Mater.*, 2015, **27**, 6317–6322.
75 B. Winther-Jensen, O. Winther-Jensen, M. Forsyth and D. R. MacFarlane, *Science*, 2008, **321**, 671–674.
76 Y. J. Li, H. C. Zhang, T. H. Xu, Z. Y. Lu, X. C. Wu, P. B. Wan, X. M. Sun and L. Jiang, *Adv. Funct. Mater.*, 2015, **25**, 1737–1744.
77 X. L. Tong, G. H. Zhao, M. C. Liu, T. C. Cao, L. Liu and P. Q. Li, *J. Phys. Chem. C*, 2009, **113**, 13787–13792.
78 C. Tang, R. Zhang, W. B. Lu, Z. Wang, D. N. Liu, S. Hao, G. Du, A. M. Asiri and X. P. Sun, *Angew. Chem., Int. Ed.*, 2017, **56**, 842–846.
79 J. X. Feng, H. Xu, S. H. Ye, G. F. Ouyang, Y. X. Tong and G. R. Li, *Angew. Chem., Int. Ed.*, 2017, **56**, 8120–8124.
80 S. Cherevko and C. H. Chung, *Electrochim. Acta*, 2010, **55**, 6383–6390.
81 Z. Lu, W. W. Xu, W. Zhu, Q. Yang, X. D. Lei, J. F. Liu, Y. P. Li, X. M. Sun and X. Duan, *Chem. Commun.*, 2014, **50**, 6479–6482.
82 L. Xu, Q. Q. Jiang, Z. H. Xiao, X. Y. Li, J. Huo, S. Y. Wang and L. M. Dai, *Angew. Chem., Int. Ed.*, 2016, **55**, 5277–5281.
83 L. L. Feng, G. T. Yu, Y. Y. Wu, G. D. Li, H. Li, Y. H. Sun, T. Asefa, W. Chen and X. X. Zou, *J. Am. Chem. Soc.*, 2015, **137**, 14023–14026.
84 X. J. Liu, Z. Chang, L. Luo, T. H. Xu, X. D. Lei, J. F. Liu and X. M. Sun, *Chem. Mater.*, 2014, **26**, 1889–1895.
85 Z. Y. Lu, M. Sun, T. H. Xu, Y. J. Li, W. W. Xu, Z. Chang, Y. Ding, X. M. Sun and L. Jiang, *Adv. Mater.*, 2015, **27**, 2361–2366.
86 K. Akbar, J. H. Kim, Z. Lee, M. Kim, Y. Yi and S. H. Chun, *NPG Asia Mater.*, 2017, **9**, e378.
87 Y. Kuang, G. Feng, P. S. Li, Y. M. Bi, Y. P. Li and X. M. Sun, *Angew. Chem., Int. Ed.*, 2016, **55**, 693–697.
88 X. Chen, Y. C. Wu, B. Su, J. M. Wang, Y. L. Song and L. Jiang, *Adv. Mater.*, 2012, **24**, 5884–5889.
89 W. J. Li, J. J. Zhang, Z. X. Xue, J. M. Wang and L. Jiang, *ACS Appl. Mater. Interfaces*, 2018, **10**, 3076–3081.
90 Y. M. Zheng, H. Bai, Z. B. Huang, X. L. Tian, F. Q. Nie, Y. Zhao, J. Zhai and L. Jiang, *Nature*, 2010, **463**, 640–643.
91 J. Ju, H. Bai, Y. M. Zheng, T. Y. Zhao, R. C. Fang and L. Jiang, *Nat. Commun.*, 2012, **3**, 1247.
92 J. Ju, K. Xiao, X. Yao, H. Bai and L. Jiang, *Adv. Mater.*, 2013, **25**, 5937–5942.
93 K. Li, J. Ju, Z. X. Xue, J. Ma, L. Feng, S. Gao and L. Jiang, *Nat. Commun.*, 2013, **4**, 2276.
94 J. Ju, Y. M. Zheng and L. Jiang, *Acc. Chem. Res.*, 2014, **47**, 2342–2352.
95 R. Ma, J. M. Wang, Z. J. Yang, M. Liu, J. J. Zhang and L. Jiang, *Adv. Mater.*, 2015, **27**, 2384–2389.
96 C. M. Yu, X. B. Zhu, K. Li, M. Y. Cao and L. Jiang, *Adv. Funct. Mater.*, 2017, **27**, 1701605.
97 R. X. Xu, X. Y. Xu, M. H. He and B. Su, *Nanoscale*, 2018, **10**, 231–238.
98 X. Tang, H. R. Xiong, T. T. Kong, Y. Tian, W. D. Li and L. Q. Wang, *ACS Appl. Mater. Interfaces*, 2018, **10**, 3029–3038.
99 X. Z. Xue, R. X. Wang, L. W. Lang, J. M. Wang, Z. X. Xue and L. Jiang, *ACS Appl. Mater. Interfaces*, 2018, **10**, 5099–5106.
100 C. M. Yu, M. Y. Cao, Z. C. Dong, J. M. Wang, K. Li and L. Jiang, *Adv. Funct. Mater.*, 2016, **26**, 3236–3243.
101 X. Z. Xue, C. M. Yu, J. M. Wang and L. Jiang, *ACS Nano*, 2016, **10**, 10887–10893.
102 C. M. Yu, M. Y. Cao, Z. C. Dong, K. Li, C. L. Yu, J. M. Wang and L. Jiang, *Adv. Funct. Mater.*, 2016, **26**, 6830–6835.
103 J. W. Chen, Y. M. Liu, D. W. Guo, M. Y. Cao and L. Jiang, *Chem. Commun.*, 2015, **51**, 11872–11875.
104 H. C. Yang, J. W. Hou, L. S. Wan, V. Chen and Z. K. Xu, *Adv. Mater. Interfaces*, 2016, **3**, 1500774.
105 H. Y. Ma, M. Y. Cao, C. H. Zhang, Z. L. Bei, K. Li, C. M. Yu and L. Jiang, *Adv. Funct. Mater.*, 2018, **28**, 1705091.

